Electrical conductivity and complex impedance analysis of La0.7-xNdxSr0.3Mn0.7Ti0.3O3 (x≤0.30) perovskite

Amel Abassi, Nabil Kallel, Sami Kallel, Kamel Khirouni, Octavio Peña

Electrical conductivity and complex impedance analysis of $La_{0.7-x}Nd_xSr_{0.3}Mn_{0.7}Ti_{0.3}O_3$ ($x \leq 0.30$) perovskite

Amel Abassi[a,*], Nabil Kallel[a], Sami Kallel[a], Kamel Khirouni[b], Octavio Peña[c]

[a]Laboratoire Physico-chimie des Matériaux, Département de Physique, Faculté des Sciences de Monastir, Université de Monastir, 5019, Tunisia.

[b]Laboratoire de Physique des Matériaux et des Nanomatériaux Appliquée à l'Environnement, Faculté des Sciences de Gabès cité Erriadh, 6079 Gabès, Université de Gabès, Tunisia.

[c]Institut des Sciences Chimiques de Rennes, UMR 6226-CNRS, Université de Rennes 1, 35042 Rennes Cedex, France.

Abstract

Polycrystalline samples $La_{0.7-x}Nd_xSr_{0.3}Mn_{0.7}Ti_{0.3}O_3$ (x= 0.10; 0.20 and 0.30) were prepared by a high-temperature solide-state reaction technique. The X-ray diffraction shows that all the samples crystallize in the orthorhombic structure, Pbnm space group, with presence of a minor unreacted Nd_2O_3. The electrical response was studied by impedance complex spectroscopy over a broad frequency range (40-100MHz) at room temperature. The values of ac conductivity for all samples were fitted by the Jonscher law $\sigma(\omega) = \sigma_{dc} + A\omega^s$. For x= 0.10 and 0.20, hopping occurs between neighboring sites, whereas for x=0.30 the hopping process occurs through longer distance. Complex impedance plots exhibit semicircular arcs described by an electrical equivalent circuit, which indicates that the Nd-doped compounds obey a non-Debye relaxation process.

Keywords: Perovskite, ac conductivity, Impedance spectroscopy, Relaxation phenomena

* Corresponding author. Tel.: +216 21 204 532.
E-mail address: abassiamel@outlook.fr (A. Abassi)

1. Introduction

Oxides with general formula ABO_3 are classified as perovskite-type oxides. These materials exhibit interesting properties giving potential applications. Several works have reported in recent years the dielectric properties of inorganic materials, such as the $CaCu_3T_3O_{12}$ [1] and Sr_2TiMnO_6 [2] perovskite ceramics. Recently, hole-doped La-based manganites such as $La_{1-x}Ca_xMnO_3$ [3], $La_{1-x}Sr_xMnO_3$ [4] and $La_{0.7}Sr_{0.3}Mn_{0.7-x}Ti_xO_3$ [5] have been investigated by alternating current (ac) and direct current (dc) transport technique.

In this context, we have previously studied the perovskite manganese oxides $La_{1-x}Sr_xMnO_3$ (LSMO) as a typical mixed-valence system because of their high electrical conductivity [6, 7], their rich physical properties and their potential applications on a wide range of electronic devices such as capacitors, sensors and photocatalysis [8-10]. Since the conductivity of LSMO is controlled by the doping element; a way to investigate the conductivity mechanism is to study the electrical properties with different dopant concentrations. In this system, a lower charge of the A-site is compensated by hole formation in the transition metal d-band. Due to lattice distortion the holes are generally localized as small polarons, responsible of electronic transport by thermally activated hopping. The electrical conduction in these materials has contributions from grains (bulk), grain boundaries, and electrode specimen interface [11, 12]. In order to understand the conduction behavior, it is necessary to separate these various contributions to the total observed resistance. Complex impedance spectroscopy (CIS) is the most reliable and important technique to study such electrical properties and processes in these materials. The CIS technique is based on analyzing the ac response of a system, and evaluation of the impedance and related parameters as a function of temperature and frequency [13, 14]. For a polycrystalline sample, this technique enables to separate the contributions of grain and grain boundaries very easily [15–17].

The purpose of the present paper is to study the effect of Nd doping on the structural, conductivity and complex impedance properties of the $La_{0.7-x}Nd_xSr_{0.3}Mn_{0.7}Ti_{0.3}O_3$ samples with x= 0.10, 0.20 and 0.30, over a wide range of frequencies at room temperature. In our polycrystalline sample $(La^{3+}_{0.7-x}Nd^{3+}_{x}Sr^{2+}_{0.3})(Mn^{3+}_{0.7}Ti^{4+}_{0.3})O_3$, Ti^{4+} ion is non-magnetic; there are no interaction between Ti^{4+} and Mn^{3+}. Also note in this context, that the absence of the mixed valence state (Mn^{3+}-Mn^{4+}) excludes the double-exchange interaction.

2. Experimental details

Polycrystalline samples of nominal composition $La_{0.7-x}Nd_xSr_{0.3}Mn_{0.7}Ti_{0.3}O_3$ with $0 \leq x \leq 0.30$ were prepared using the conventional solid state reaction method. The details of the preparation procedure have been reported elsewhere [18]. Identification of the phase and structural analysis were carried out by ″PaNalytical X'Pert Pro″ diffractometer with filtered (Ni filter) Cu radiation ($\lambda_{CuK\alpha 1}$=1.5406 Å) in the Bragg angle range $20^{\circ} \leq 2\theta \leq 120^{\circ}$. The data were analyzed using the Rietveld method [18].

For the electrical measurements, the opposite sides of the sample were coated with conducing silver paint. The transport properties of the polycrystalline sample were examined by ac impedance spectroscopy using an Agilent 4294A over a frequency range from 40-100 MHz at room temperature.

3. Results and discussion

3.1. Structural analysis

The microstructure and their composition analysis of specimens were studied by scanning electron microscopy (SEM) on a JSM-6400 apparatus working at 20 kV at room temperature with an energy dispersive X-ray spectrometer (EDX). The EDX spectra at room temperature of $La_{0.7-x}Nd_xSr_{0.3}Mn_{0.7}Ti_{0.3}O_3$ (x=0.10; 0.20 and 0.30) samples are shown in Fig. 1. These spectra reveal that, besides the presence of La, Nd, Sr, Mn and Ti elements, no other elements were introduced in the samples during their elaboration, this indicates that the obtained chemical compositions are close to the nominal ones used for synthesis (La: Nd: Sr: Mn: Ti = (0.70-x): x: 0.30: 0.70:0.30), within the accuracy limits of the analysis (x± 0.01) [18].

The polycrystalline $La_{0.70-x}Nd_xSr_{0.30}Mn_{0.70}Ti_{0.30}O_3$ compounds were characterized by X-ray diffraction (XRD) at room temperature in a previous work [18]. These compounds crystallize in the orthorhombic structure with Pbnm space group with minor Nd_2O_3 impurities which were refined as a secondary phase. After several trials using different sintering conditions, this secondary phase still persisted, attaining a maximum value of 3.59 % wt.%, for x = 0.20.

We have used the Williamson-Hall approach to deconvolute the crystallite size and the strain contribution to the X-ray line broadening since the Scherrer's formula [19] is not appropriate to evaluate any strain contribution. In this approach, the X-ray line broadening comes from the contribution of small crystallite sizes and the broadening caused by the lattice strain [20, 21].

$\beta_{hkl} = \beta_{size} + \beta_{strain}$ (1)

where $\beta_{Size} = \frac{k\lambda}{D\cos\theta}$ (from Scherrer's formula) [19]

with λ, the X-ray wavelength (Cu Kα radiation, λ=1.5406 Å), θ the diffraction angle of the most intense peak $((hkl) \equiv (112))$ and β the breadth of the observed diffraction line at its half intensity maximum; k is the so-called shape factor, which usually takes a value of about 0.9.

The contribution of the lattice strain can be evaluated through:

$\beta_{strain} = 4\varepsilon \tan\theta$, where ε is the strain $\left(\frac{\Delta l}{l}\right)$,

Therefore Eq. (1) becomes: $\beta_{hkl} = \frac{k\lambda}{D\cos\theta} + 4\varepsilon \tan\theta$

By rearranging the above equation, we get: $\beta_{hkl}\cos\theta = \frac{k\lambda}{D} + 4\varepsilon \sin\theta$

Fig.2 shows the Williamson-Hall plot for the sample with x= 0.10. The slope of the plot $\beta_{hkl}\cos\theta$ vs. $4\sin\theta$ gives the value of the micro-strain whereas the intercept results yields the crystallite size. The crystallite size (D) and the strain (ε) are listed in table 1.

In the Williamson–Hall method, the broadening due to strain is completely removed and so the crystallite size is larger when compared to the results observed by the Debye–Scherer method [22]. The strain decreases with increasing Nd-doping (Table1). The strain in the diffracting planes originates from micro-stresses caused by structural imperfections which may be related to the grain size [23].

The variation of the X-ray density (theoretical density), apparent density (experimental density) and porosity p with Nd^{3+} concentration (x) are also reported in table 1. The X-ray density was calculated using the formula [24]:

$$\rho_{th} = \frac{ZM}{N_a V} \quad (2)$$

where, Z is the number of molecules per unit cell of the orthorhombic structure, M is the molecular weight of the sample, N_a is the Avogadro's number, V is the volume for a orthorhombic unit cell. The experimental density of the samples was calculated using the formula [24]:

$$\rho_{exp} = \frac{m}{\pi r^2 h} \quad (3)$$

where m, r and h are respectively the mass, radius and the thickness of the samples. The percentage porosity was calculated using the relation [24]:

$$p = \left(1 - \frac{\rho_{\exp}}{\rho_{th}}\right) \text{x } 100 \qquad (4)$$

From table 1, the apparent density of the samples was found smaller than the X-ray density (theoretical density), which may be due to the existence of pores, which in turn, depends on the sintering conditions. Indeed, during uniaxial pressing of these ceramic powder particles, some pores or void spaces are created. During initial sintering, a grain boundary forms between adjacent particles and every interstice becomes a pore. The value of the percentage porosity of the samples was found in the range 12 to 17% (see table1).

3.2. Electrical conductivity analysis

The frequency dependence of the ac conductivity for $La_{0.7-x}Nd_xSr_{0.3}Mn_{0.7}Ti_{0.3}O_3$ (x=0.10, 0.20 and 0.30) at room temperature is shown in Fig. 3. The ac conductivity can be splitted into two parts. Firstly, in the frequency range between 40 to 3×10^5 Hz, the conductivity is practically constant (as shown by a plateau). This plateau corresponds to the dc-conductivity. Secondly, at higher frequencies, the variation ac conductivity occurs with changes in slope and progressively increases with increasing frequency, suggesting a superposition of different transport mechanisms. Different types of hopping and carrier species are then involved in the transport behavior. The conductivity can be described by the Jonscher power law [25-27]:

$$\sigma(\omega) = \sigma_{dc} + A\omega^s \qquad (5)$$

where σ_{dc} is the dc-conductivity, A is a pre-exponential factor and s is the frequency exponent which may be found by a non-linear fit of the conductivity graphs.

The value of s has a physical meaning: if $s \leq 1$, the hopping motion involves a translation motion with a sudden hopping whereas, if $s > 1$, the hopping motion involves localized hopping between neighboring sites. The values of s are obtained from equation (5) and the best fit to the experimental data, and are plotted as a function of the Nd content in the inset Fig. 3. It is clear that the conductivity decreases with increasing Nd concentration, due to a disorder introduced by a size mismatch between La and Nd ions. Indeed, the smaller ionic radius of Nd compared to La produces a decrease of $\langle r_A \rangle$ and a decrease of the (Mn/Ti)-O-(Mn/Ti) bond angle which causes a narrowing of the bandwidth. This behavior is confirmed by the electrical resistivity ρ(T) measurements reported in our previous paper [18].

From the inset Fig. 3, it is seen that the value of s slightly decreases with increasing of Nd content: for samples with x ≤ 0.20 the values of s are slightly higher than 1 (Table 2), which indicates that the hopping occurs between neighboring sites [28]. However, for x=0.30, the value of the s-parameter is found to 0.92; it can then be expected that the polarizability of the material depends on the energy barrier for a simple hopping process between two sites [29]. Recent reports also discuss the ac response of materials in connection to the nature and value of the s parameter [30, 31].

The ac conductivity data have been used to evaluate the density of states at the Fermi level $N(E_f)$ using the relation [32]:

$$\sigma_{AC}(\omega) = \frac{\pi}{3} e^2 \omega k_B T \left\{N(E_f)\right\}^2 \alpha^{-5} \left\{\ln\left(\frac{f_0}{\omega}\right)\right\}^4 \qquad (6)$$

where e is the electronic charge, f_0 the photon frequency and α the localized wave function, and assuming $f_0 = 10^{13}$ Hz [33, 34] and α = 2.22 nm^{-1} [35]. Fig. 4 shows the frequency dependence of $N(E_f)$ for $La_{0.7-x}Nd_xSr_{0.3}Mn_{0.7}Ti_{0.3}O_3$ (x= 0.10, 0.20, 0.30). The density of states $N(E_f)$ decreases exponentially with the increase in frequency. The power law dependence of the ac conductivity with frequency corresponds to the short-range hopping of carriers through trap sites separated by an energy barrier of various heights. Grain boundaries are formed during the sintering process in porous materials due to surface reduction or oxidation of crystallites due to their direct contact with the firing atmosphere. Presence of small grains implies an increased number of insulating grain boundaries and hence, increased energy barriers to conduction electrons.

3.3 Complex impedance analysis

Impedance spectroscopy is an experimental technique for the characterization of electrical properties of electronic materials, such as conductivity, dielectric behavior, relaxation characteristic, etc. Fig. 5 shows the complex impedance spectra of $La_{0.7-x}Nd_xSr_{0.3}Mn_{0.7}Ti_{0.3}O_3$ (x =0.10, 0.20 and 0.30) at room temperature. The impedance spectra are characterized by the appearance of semicircle arcs, which can be well traced with the increase of frequency. The presence of a single semicircular arc indicates that the electrical processes in the material arise basically due to the contribution from bulk material [36-38]. These semicircular arcs are off-centered, as it can be seen in Fig. 5, and therefore reflect a non-Debye type relaxation process for all our Nd-doped compounds [33, 39-42].

The impedance results were fitted using Z-view software. The best fits are obtained when we use an equivalent circuit involving a serial association of a grain resistance R_g (bulk resistance) with a resistance R_{gb} (grain-boundary resistance) associated in parallel with constant phase element impedance (Z_{CPE}). The equivalent circuit formed by $R_g + (R_{gb}//Z_{CPE})$, is shown in the inset Fig. 5. The intersect of the semicircle with the real axis at low frequencies is ascribed to the total resistance $R_T = R_g + R_{gb}$. On the other hand, the impedance response R_g of the grain dominates at high frequencies and its value can be deduced from the left intersect of the semicircle with real axis. Then, R_{gb} is given by $R_{gb} = R_T - R_g$.

The CPE impedance (Z_{CPE}) is given by the following relation:

$$Z_{CPE} = \left[A_0 (j\omega)^{\alpha}\right]^{-1} \tag{7}$$

where α ($0 < \alpha < 1$) is the exponent which determines a constant phase angle equal to ($\alpha\pi/2$), $\omega = 2\pi f$ is the angular frequency, $j^2 = -1$ and A_0 is the CPE parameter (expressed in Farad units). For an α value equal to 1, 0.5 or 0, CPE will be, respectively, an ideal capacitance, a Warburg impedance or an ideal resistance. A_0 and α can be temperature-dependent.

The expression of real (Z') and imaginary (Z") components of the impedance related to the equivalent circuit can be expressed by the following relationships:

$$Z' = R_g + \frac{R_{gb}(1 + R_{gb}A_0\omega^{\alpha}\cos(\frac{\alpha\pi}{2}))}{(1 + R_{gb}A_0\omega^{\alpha}\cos(\frac{\alpha\pi}{2}))^2 + (R_{gb}A_0\omega^{\alpha}\sin(\frac{\alpha\pi}{2}))^2} \tag{8}$$

$$Z'' = \frac{R_{gb}^{\ 2}A_0\omega^{\alpha}\sin(\frac{\alpha\pi}{2}))}{(1 + R_{gb}A_0\omega^{\alpha}\cos(\frac{\alpha\pi}{2}))^2 + (R_{gb}A_0\omega^{\alpha}\sin(\frac{\alpha\pi}{2}))^2} \tag{9}$$

The parameters R_g, R_{gb}, A_0 (CPE) and α have been obtained by a mean square method used to minimize the difference between the experimental and calculated data. The parameters are listed in table 3.

It is usually found that the grain boundary resistance is generally higher in these manganites as compared to the conducting grains. This is ascribed to the fact that the atomic arrangement near the grain boundary region is disordered, resulting in a serious increase of the electron scattering. In addition, the internal space-charge created at the grain boundaries may lead to a significant increase in the concentration of mobile charges [26,43]. As expected,

the resistance R_{gb} increases with the concentration x, indicating a decrease of the electrical conductivity (σ_{dc}).

Fig. 6 shows the imaginary (Z") component of the impedance as a function of frequency, at room temperature, for x = 0.10, 0.20 and 0.30. A single peak is observed at a frequency f_r. From these peaks we may deduce the value of the relaxation frequency (f_r) and we can calculate the relaxation time (τ_{cc}) using the relation $\tau_{cc} = (2\pi f_r)^{-1}$. This behavior similar to the one obtained in our previous work [5, 17], describes the type and strength of the electrical relaxation phenomenon [44-46] and indicates the presence of relaxation processes in the material.

To analyze the relaxation process, we interpreted the impedance data considering a distribution of relaxation times. Therefore, considering the relaxation time τ_{cc}, we can write:

$$Z^*(\omega) = Z_\infty + (Z_0 - Z_\infty)\int_0^{+\infty}(1+ j\omega\tau_{cc})^{-1}G(\tau)d(\tau) \qquad (10)$$

Here, $G(\tau)$ is the distribution function of time constants, and $G(\tau)d(\tau)$ is the probability of finding a Debye element in the differential time element. The distribution must be normalizable,

$$\int_0^{+\infty} G(\tau)d\ln(\tau) = 1 \qquad (11)$$

For the Cole-Cole model, the derived distribution function is given by the following equation [47, 48]:

$$G(\tau) = \frac{1}{2\pi}\frac{\sin(\alpha\pi)}{\cosh[(1-\alpha)\log(\tau/\tau_{cc})] - \cos(\alpha\pi)} \qquad (12)$$

In Fig. 7 we present the calculated distribution functions for different Nd concentrations around f_r (f $>10^3$ KHz). The Cole–Cole distribution, like the lognormal distribution, is symmetrical with respect to a central frequency or relaxation time. The distribution function of relaxation time is plotted as a function of the variable $\log(\tau/\tau_{cc})$ in Fig. 7, confirmed this behavior. This can represent a relaxation process associated with point defects, such as trapping and de-trapping of electrons in deep traps in the grain or in depletion layer regions adjoining the grain boundary.

Generally, this kind of properties depends on the sample parameters, such as thickness and morphology, series resistance and density of the interface states between grains. Grain

boundaries contain defects which can cause positive or negative space charge distribution at the interfaces between the particles. Under the application of an external field, the space charges can move and, when they are trapped by the defects, many dipole moments (space charge polarization) can be formed, resulting in decentered semi-circles on the real axis.

The decrease in conductivity confirms this behavior. The non-Debye character of the relaxation processes is obvious. The impedance results obtained have confirmed this behavior. Similar behavior is observed in many other works [46, 48].

4. Conclusion

In summary, in this work we have investigated the structure and electrical transport properties of $La_{0.7-x}Nd_xSr_{0.3}Mn_{0.7}Ti_{0.3}O_3$ (x= 0.10, 0.20 and 0.30) perovskites over a broad frequency range (40-100MHz) at room temperature. Rietveld analysis revealed that all samples contained of a minor unreacted Nd_2O_3 phase with orthorhombic Pbnm symmetry. It was found that Nd substitution affects the ac conductivity and the impedance study. The electrical conductivity obeys the Jonscher universal power law. The hopping process occurs between neighboring sites for x= 0.1 and 0.2 and through long distance hopping for x=0.3. The complex impedance analysis indicates that the electrical properties of the materials are strongly dependent on frequency. The impedance study using Nyquist representation revealed the appearance of decentered semicircle arcs, indicating the existence of a relaxation time distribution, well modeled in terms of an electrical equivalent circuit. Distribution functions of the relaxation times confirmed this behavior.

5. References

[1] M. A. Subramanian, D. Li, N. Duan, B. A. Reisner, A.W. Sleight, J. Solid. State. Chem. 151 (2000) 323-325.

[2] K. R. S. Preethi Meher, K. B. R. Varma, J. Appl. Phys. 105 (2009) 034113.

[3] J. L. Cohn, M. Peterca, J. J. Neumeier, Phys. Rev. B 70 (2004) 214433.

[4] A. Pimenov, Ch. Hartinger, A. Loidl, A. A. Mukhin, V.Yu. Ivanov, A. M. Balbashov, Phys. Rev. B 59 (1999) 12419.

[5] H. Rahmouni, M. Nouiri, R. Jemai, N. Kallel, F. Rzigua, A. Selmi, K. Khirouni, S. Alaya, J. Magn. Magn. Mater. 316 (2007) 23-28.

[6] K. Sakthipandi, V. Rajendran, T. Jayakumar, Mater. Res. Bull. 48 (2013) 651.

[7] H. Jian, Z. Zhang, Y. Wang, X. Tang, J. Yang, L. Hu, Li Chen, X. Zhu, Y. Sun, J. Alloys Compd. 561 (2013) 95-100.

[8] R. J. Cava, J. Mater. Chem. 11 (2001) 54-62.

[9] Leandro da Conceição, L. Dessemond, E. Djurado, M. M.V. M. Souza, J. Power Sources, 241 (2013) 159-167.

[10] G. Wang, Z. D. Wang, L. D. Zhang, Mater. Sci. Eng. B 116 (2005) 183.

[11] I. M. Hodge, M. D. Ingram, A. R. West, J. Electroanal. Chem. 74 (1976) 125-143.

[12] C.Y. Hsu, Hsiung Chou, B.Y. Liao, J.C.A. Huang, Appl. Phys. Lett. 89 (2006) 262501.

[13] M. A. L. Nobre, S. Lanfredi, J. Phys. Condens. Matter 12 (2000) 7833-7841.

[14] M. A. L. Nobre, S. Lanfredi, Mater. Lett. 47 (2001) 362-366.

[15] N. Sdiri, R. Jemai, M. Bejar, M. Hussein, K. Khirouni, E. Dhahri, S. Mazen, Solid State Commun. 148 (2008) 577-581.

[16] M. Nadeem, M. J. Akhtar, M. N. Haque, Solid State Commun. 145 (2008) 263–266.

[17] S. Kallel, A. Nasri, N. Kallel, H. Rahmouni, O. Peña, K. Khirouni, M. Oumezzine, Physica B 406 (2011) 2172-2176.

[18] A. Abassi, N. Kallel, S. Kallel, O. Peña, J. Supercond Nov Magn. 27 (2014) 2353-2364.

[19] A. Guinier, "Théorie et Technique de la Radiocristallographie", 3^{éme} édition, Dunod (1964) 462.

[20] V. Eswaramoorthi, R. Victor Williams, J. ceramint. 41 (2015) 2434-2438.

[21] P. Goel, K. L. Yadav, J. Mater. Sci. 42 (2007) 3928-3935.

[22] S. Eitssayeam, U. Intatha, K. Pengpat, G. Rujijanagul, K. J. D. MacKenzie, T. Tunkasiri, Curr. Appl. Phys, 9 (2009) 993-996.

[23] Y. H. Zhao, U. Welzel, J.V. Lier, E. J. Mittemeijer, Thin Solid Films 514 (2006) 110-119.

[24] K. M. Batoo, S. Kumar, C. G. Lee, Alimuddin, Curr. Appl. Phys. 9 (2009) 826-832.

[25] S. Lanfredi, P.S. Saia, R. Lebullenger, Solid State Ionics 146 (2002) 329-339.

[26] A. K. Jonscher, Universal Relaxation Law, Chelsea Dielectric Press, London, 1996.

[27] A. K. Jonscher, Dielectric Relaxation in Solids, Chelsea Dielectric Press, London, 1983.

[28] Banerji Behera, P. Nayak, R. N. P. Choudhary, J. Alloys Compd. 436 (2007) 226.

[29] A. Pelaiz-Barranco, M. P. Gutierrez-Amador, A. Huanosta, R. Valenzuela, Appl. Phys. Lett. 73 (1998) 2039-2041.

[30] S. Khadhraoui, A. Triki, S. Hcini, S. Zemni, M. Oumezzine, J. Alloys Compd. 574 (2013) 290-298.

[31] A. Omri, M. Bejar, E. Dhahri, M. Es-Souni, M. A. Valente, M. P. F. Graça, L. C. Costa, J. Alloys Compd. 536 (2012) 173-178.

[32] I.G. Austin, N.F. Mott, Adv. Phys. 18 (1969) 41.

[33] Lily, K. Kumari, K. Prasad, R.N.P. Choudhary, J. Alloys Compd 453 (2008) 325-331.

[34] G. Zhang, H. Chen, Y. Xiea, F. Huang, Cryst. Eng. Comm, 16 (2014) 1810-1816.

[35] D. Emin, T. Holstein, Phys. Rev. B 13, 647 (1976).

[36] J. T. C. Irvine, D. C. Sinclair, A. R. West, Electroceramics: Characterization by Impedance Spectroscopy, Adv. Mater. 2 (1990) 132–138.

[37] S. Selvasekarapandian, M. Vijaykumar, Mater. Chem. Phys. 80 (2003) 29–33.

[38] Shrabanee Sen, R. N. P. Choudhary, Mater. Chem. Phys. 87 (2004) 256e263.24

[39] P. Dhak, D. Dhak, M. Das, K. Pramanik, P. Pramanik, Mater. Sci. Eng. B 164 (2009) 165-171.

[40] V. Prakash, A. Dutta, S. N. Choudhary, T. P. Sinha, Mater. Sci. Eng. B 142 (2007) 98-105.

[41] U. Intatha, S. Eitssayeam, J. Wang, T. Tunkasiri, Curr. Appl. Phys. 10 (2010) 21-25.

[42] S. Sen, S. K. Mishra, S. S. Palit, S. K. Das, A. Tarafdar, J. Alloys Compd. 453 (2008) 395-400.

[43] J. R. Macdonald, Impedance Spectroscopy Theory, Experiment, and Applications, John Wiley & Sons, (2005).

[44] P. T. Phong, B. T. Huy, Y. -I. Lee, I. -J. Lee, J. Alloys Compd 583 (2014) 237-243

[45] S. Pattanayak , B. N. Parida, Piyush R. Das, R. N. P. Choudhary, Appl Phys A 112 (2013) 387-395.

[46] N. Chihaoui, M. Bejar, E. Dhahri, M. A.Valente, M. P. F.Graça, L. C. Costa, J. Alloys Compd. 577S (2013) S483-S487.

[47] S. N. Al-Refaie, Appl. Phys. A 52 (1991) 234-236.

[48] L. C. Costa, M. E. Achour, M. P. F. Graça, M. El Hasnaoui, A. Outzourhit, A. Oueriagli, J. Non-Cryst. Sol. 356 (2010) 270-274.

Fig.1: The EDX analysis spectrum at room temperature of $La_{0.7-x}Nd_xSr_{0.3}Mn_{0.7}Ti_{0.3}O_3$ (x=0.10; 0.20 and 0.30) compound.

Fig.2: Williamson-Hall plot for $La_{0.6}Nd_{0.1}Sr_{0.30}Mn_{0.70}Ti_{0.30}O_3$.

Fig.3: Variation of the ac conductivity (σ_{AC}) as a function of frequency, measured at room temperature. The solid lines are the fits obtained using Eq. (5). The inset shows the variation of the exponent s with the Nd concentration for $La_{0.7-x}Nd_xSr_{0.3}Mn_{0.7}Ti_{0.3}O_3$.

Fig.4: Frequency dependence of $N(E_F)$ for $La_{0.7-x}Nd_xSr_{0.3}Mn_{0.7}Ti_{0.3}O_3$ (x=0.10, 0.20, 0.30) samples at room temperature.

Fig.5: Complex impedance for $La_{0.7-x}Nd_xSr_{0.3}Mn_{0.7}Ti_{0.3}O_3$ (x =0.10, 0.20, 0.30) measured at room temperature. The inset shows the equivalent circui.

Fig.6: Variation of imaginary part (Z'') of impedance for $La_{0.7-x}Nd_xSr_{0.3}Mn_{0.7}Ti_{0.3}O_3$ (x =0.10; 0.20 and 0.30) with frequency at room temperature. Inset shows the variation of reel part (Z')

Fig.7: Distribution function of relaxation times for given Nd concentrations of the $La_{0.7-x}Nd_xSr_{0.3}Mn_{0.7}Ti_{0.3}O_3$ system.

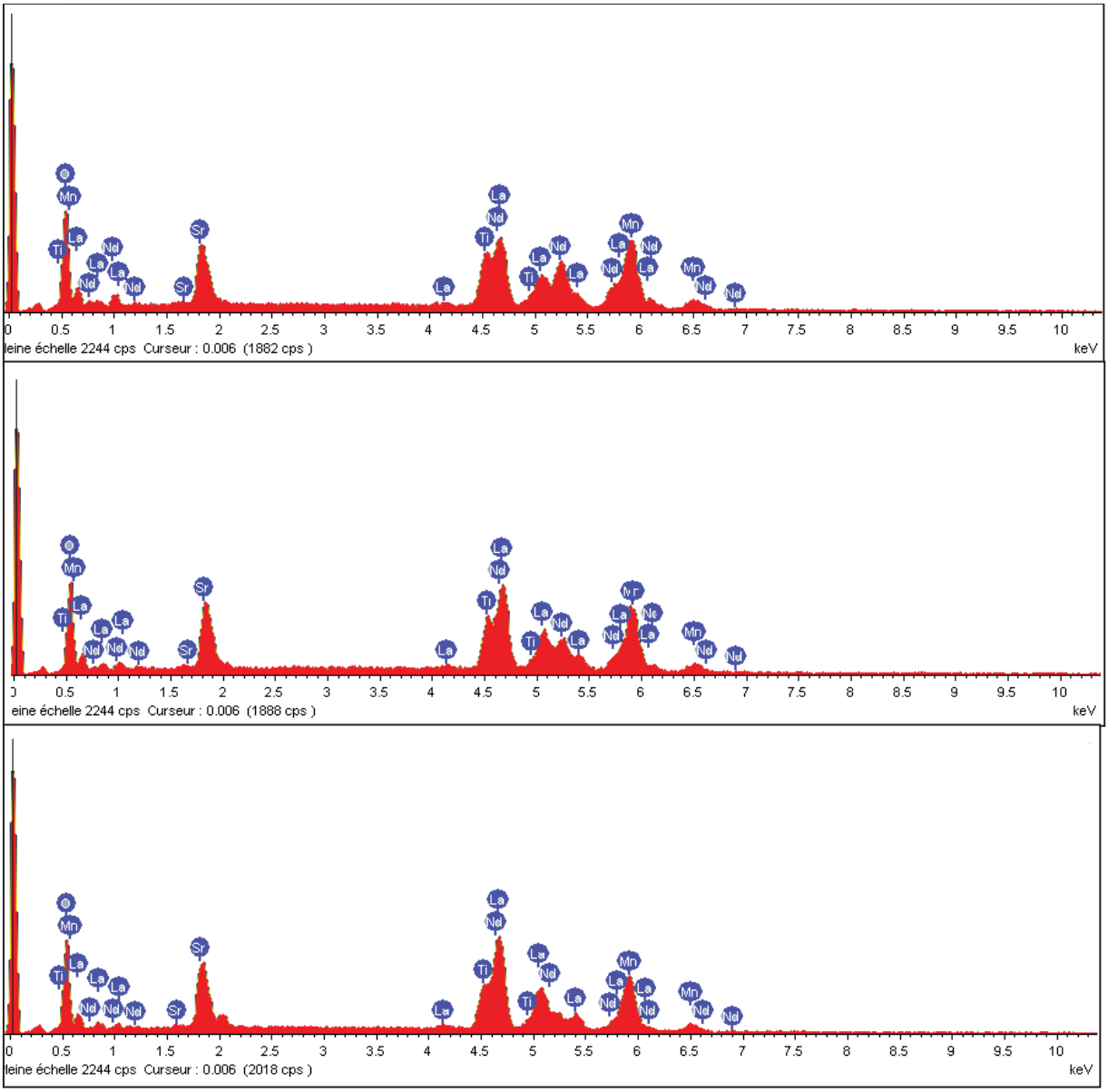

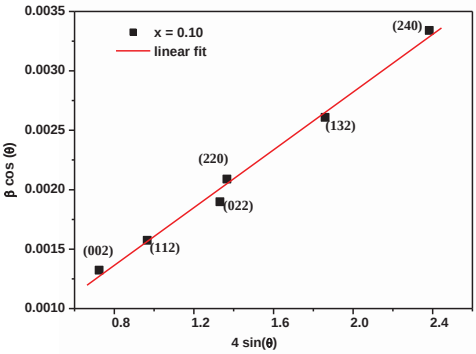

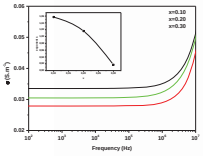

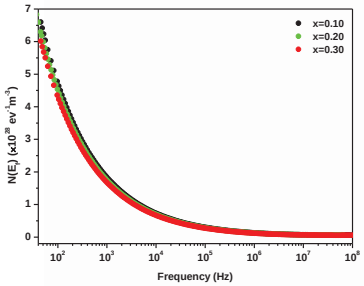

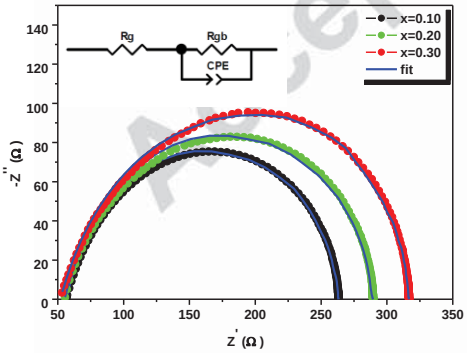

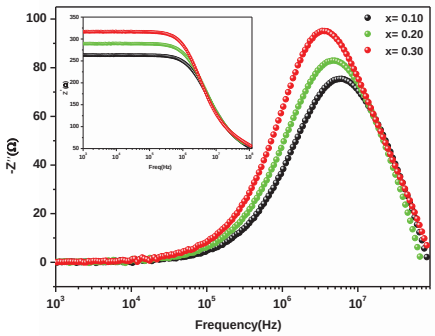

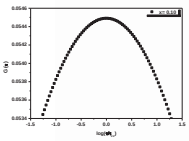

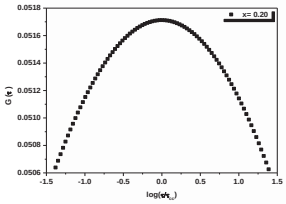

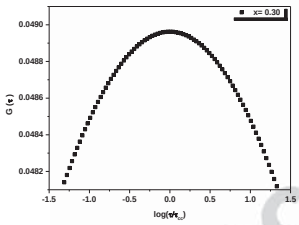

	ρ_{exp} (g cm^{-3})	ρ_{th} (g cm^{-3})	p (%)	Strain (ε) %	Average crystallite size	
					Debye-Scherrer technique (D_S) (nm)	Williamson-Hall technique (D) (nm)
x= 0.10	5.452	6.206	12.1	1.07×10^{-3}	108	274
x= 0.20	5.305	6.283	15.5	9.76×10^{-4}	111	359

x= 0.30	5.226	6.288	16.8	9.48×10^{-4}	110	301

Table 1: Values of ρ_{th}, ρ_{exp}, p, strain and crystallite size of samples $La_{0.7-x}Nd_xSr_{0.3}Mn_{0.7}Ti_{0.3}O_3$, prepared by solid state reaction.

samples	σ_{dc} (S m^{-1})	A	s
x = 0.10	0.335	7.0×10^{-10}	1.05
x = 0.20	0.300	1.4×10^{-9}	1.01
x = 0.30	0.276	6.0×10^{-9}	0.92

Table 2: Nonlinear fit of conductivity using eq. (5) from data at room temperature for samples $La_{0.7-x}Nd_xSr_{0.3}Mn_{0.7}Ti_{0.3}O_3$ (x= 0.10, 0.20, 0.30).

Sample	R_g (Ω)	R_{gb} (Ω)	CPE(F)	α
x = 0.10	56	206	9.9×10^{-6}	0.79
x = 0.20	62	227	1.7×10^{-6}	0.80
x = 0.30	60	257	4.4×10^{-7}	0.81

Table 3: Electrical parameters deduced from complex impedance fo $La_{0.7-x}Nd_xSr_{0.3}Mn_{0.7}Ti_{0.3}O_3$ (x = 0.10, 0.20, 0.30) at room temperature.

Highlights

- The $La_{0.7-x}Nd_xSr_{0.3}Mn_{0.7}Ti_{0.3}O_3$ samples crystallize in the orthorhombic structure.
- The conductivity decreases with increasing Nd concentration.
- The impedance spectra are characterized by the appearance of semicircle arcs.
- The distribution function of relaxation time presents a symmetrical shape with respect to the central frequency.